RESEARCH ARTICLE

ADVANCED ELECTRONIC MATERIALS Open Access

www.advelectronicmat.de

Phase Transformation Driven by Oxygen Vacancy Redistribution as the Mechanism of Ferroelectric $Hf_{0.5}Zr_{0.5}O_2$ Fatigue

*Zimeng Zhang, Isaac Craig, Tao Zhou, Martin Holt, Raul Flores, Evan Sheridan, Katherine Inzani, Xiaoxi Huang, Joyeeta Nag, Bhagwati Prasad, Sinéad M. Griffin, and Ramamoorthy Ramesh**

As a promising candidate for nonvolatile memory devices, the hafnia-based ferroelectric system has recently been a hot research topic. Although significant progress has been made over the past decade, the endurance problem is still an obstacle to its final application. In perovskite-based ferroelectrics, such as the well-studied $Pb[Zr_xTi_{1-x}]O_3$ (PZT) family, polarization fatigue has been discussed within the framework of the interaction of charged defects (such as oxygen vacancies) with the moving domains during the switching process, particularly at the electrode-ferroelectric interface. Armed with this background, a hypothesis is set out to test that a similar mechanism can be in play with the hafnia-based ferroelectrics. The conducting perovskite La-Sr-Mn-O is used as the contact electrode to create $La_{0.67}Sr_{0.33}MnO_3$ / $Hf_{0.5}Zr_{0.5}O_2$ (HZO)/ $La_{0.67}Sr_{0.33}MnO_3$ capacitor structures deposited on $SrTiO_3$-Si substrates. Nanoscale X-ray diffraction is performed on single capacitors, and a structural phase transition from polar o-phase toward non-polar m-phase is demonstrated during the bipolar switching process. The energy landscape of multiphase HZO has been calculated at varying oxygen vacancy concentrations. Based on both theoretical and experimental results, it is found that a polar to non-polar phase transformation caused by oxygen vacancy redistribution during electric cycling is a likely explanation for fatigue in HZO.

1. Introduction

Hafnia-Zirconia ferroelectrics have attracted attention as promising candidates for nonvolatile memory and logic due to their robust ferroelectricity at the nanoscale thickness and compatibility with the Complementary Metal-Oxide-Semiconductor (CMOS)electronics.[1–5] However, despite their potential, limited endurance and a high coercive field (and a consequent high switching voltage) are potential limitations to widespread adoption.[6] Previous studies have demonstrated a "wake-up effect" and fatigue behavior in Hafnia-Zirconia during field cycling, with an emerging consensus built around the crucial role of oxygen vacancies.[7–11] A complete understanding of endurance behavior in Hafnia-Zirconia and its microscopic origin is therefore vital to understand how they can be improved.

Hafnia/Zirconia exist in various phases under different conditions,

Z. Zhang, X. Huang, R. Ramesh
Department of Materials Science and Engineering
University of California
Berkeley, California 94720, USA
E-mail: rramesh@berkeley.edu

I. Craig, R. Flores, E. Sheridan, S. M. Griffin
Molecular Foundry
Lawrence Berkeley National Laboratory
Berkeley, CA 94720, USA

The ORCID identification number(s) for the author(s) of this article can be found under https://doi.org/10.1002/aelm.202300877

© 2024 The Author(s). Advanced Electronic Materials published by Wiley-VCH GmbH. This is an open access article under the terms of the Creative Commons Attribution License, which permits use, distribution and reproduction in any medium, provided the original work is properly cited.

DOI: 10.1002/aelm.202300877

I. Craig
Department of Chemistry
University of California
Berkeley, California 94720, USA

I. Craig, R. Flores, E. Sheridan, S. M. Griffin
Materials Sciences Division
Lawrence Berkeley National Laboratory
Berkeley, CA 94720, USA

T. Zhou, M. Holt
Center for Nanoscale Materials
Argonne National Laboratory
Lemont, IL 60439, USA

K. Inzani
School of Chemistry
University of Nottingham
Nottingham NG7 2RD, UK

J. Nag
Western Digital Research Center
Western Digital Corporation
San Jose, CA 95119, USA

which have been previously reported extensively.[12–14] Unlike many other promising ferroelectric materials, their polar phases are in fact metastable – the ferroelectric orthorhombic phase ($Pca2_1$), and the antiferroelectric orthorhombic phase (Pbca), have only been found in thin films under certain strain/doping conditions.[13] The ground state of bulk Hafnia-Zirconia at room temperature is the non-ferroelectric monoclinic phase ($P2_1/c$). The most popular composition that can robustly achieve a polar phase is $Hf_{0.5}Zr_{0.5}O_2$ (HZO), with TiN as the top and bottom electrodes.[12,15–17] Typically, these stacks are deposited via Atomic Layer Deposition (ALD) with post-annealing used to apply the necessary mechanical stress to form the polar crystalline structure.[15] However, these ferroelectric HZO films are often polycrystalline, leading to issues with switching and endurance. In particular, endurance tests on HZO devices deposited on TiN have shown a significant wake-up effect (increasing switched polarization with cycling) at the initial 10^3 cycles and noticeable fatigue (decreasing switched polarization) at $\approx 10^7$ cycles, presenting a significant barrier for practical applications.[6,10]

We set out to probe the role of oxygen-related defects in influencing polarization fatigue by going back to the well-established literature in perovskite ferroelectrics such as $Pb[Zr_xTi_{1-x}]O_3$ (PZT), wherein conducting oxide electrodes have been shown to significantly ameliorate the loss of switchable polarization during bipolar cycling.[18–21] With this as the background and with the hypothesis that conducting oxides may also provide a similar benefit in the case of HZO, we initiated a study of the role of conducting perovskite electrodes. We deposited highly textured HZO films on a $La_{0.67}Sr_{0.33}MnO_3$ (LMSO) electrode using pulsed laser deposition (PLD). The oxide LSMO/HZO/LSMO stack, **Figure 1a**, exhibits a large polarization and has been previously studied.[22–25] We deposited the stack on STO-Si substrates, in order to both obtain highly [001] textured LSMO as well as to be consistent with Si integration. Our endurance tests on capacitor structures show an endurance up to 10^{11} cycles, which, although still short of commercial requirements, is a marked improvement compared to films on TiN.[6,10] To gain more insight into the fundamental origins of bipolar fatigue, we conducted structural measurements on fatigued devices, illustrating the intricacies of polarization switching and fatigue mechanisms in HZO. Our findings, corroborated by first-principles calculations, indicate two key mechanisms for fatigue: a reversible component due to oxygen vacancy redistribution during electronic field cycling, and an irreversible component arising from the competing phase stability of the monoclinic nonpolar phase.

The field cycling behavior of HZO (Figure 1b) shares similarities with that of lead zirconate titanate (PZT).[26–28] In particular, both exhibit a wake-up effect at the beginning of cycling, and their fatigued polarization can be recovered by the application of higher voltage pulses, Figure 1c. Such a voltage-induced recovery of switched polarization is also implicit in Figure 1b where larger voltage pulse amplitudes correlate to a longer endurance, indicating the recovery of polarization due to the higher voltage cycling pulses. On the surface, these similar behaviors of HZO and PZT suggest a possible common cause: such as domain pinning/depinning caused by defects such as oxygen vacancies. The role of domain pinning in ferroelectric wake-up and fatigue has been explored in prior studies on PZT.[26–28] Given HZO's high oxygen conductivity,[29,30] charged oxygen vacancies can migrate through the stack during electrical cycling[24] and segregate at grain boundaries and interfaces,[11] resulting in the pinning of the adjacent ferroelectric domains. Higher voltage pulses aid in the redistribution of oxygen vacancies and domain depinning, thus restoring polarization values. An alternative pathway could be one in which the insertion/removal of oxygen vacancies into the HZO lattice leads to changes in the thermodynamic stability of the polar phase. In order to study this further, we carried out a combination of ab initio theoretical calculations of the stability if the polar orthorhombic phase in conjunction with structural studies.

It is noteworthy, however, that the HZO fatigue cannot be entirely attributed to domain pinning. We find that part of the polarization cannot be recovered either by electric pulses or annealing (Figure 1c,d). Further evidence of this is shown with the permanent change of the HZO layer during fatigue in **Figure 2**. We subjected the system to repeated bi-polar electric field cycling, progressively increasing the frequency from 1 Hz to 1 MHz. We recorded the remnant polarization values as a function of the accumulated cycles. To investigate the fatigue recovery behavior, we initiated multiple cycles starting from the lowest frequency once the capacitor exhibited degradation of remnant polarization. Figure 2 illustrates the capacitor under study, which underwent seven cycles of this process, effectively demonstrating a cyclic pattern of fatigue, recovery, and subsequent fatigue. While oxygen vacancies are more responsive to low-frequency electric pulses, (allowing for polarization recovery when cycled under low frequency), the polarization eventually attains a stable value that is much lower than the initial polarization after several wake-up-fatigue cycles. This indicates a mechanism beyond domain pinning contributing to fatigue, namely an irreversible effect occurring within the HZO layer that degrades its intrinsic ferroelectricity. We therefore proceeded to carry out theoretical calculations and structural measurements to probe the origins of this behavior.

First, we performed Density Functional Theory (DFT) calculations to explore the role of oxygen vacancies on the phase stability of the polar and nonpolar phases of HZO. We considered the antiferroelectric (o-AFE) and ferroelectric (o-FE) polymorphs with space groups Pbca and $Pca2_1$ respectively, the nonpolar monoclinic phase (m) with space group $P2_1/c$, and the presumed nonpolar parent/intermediate tetragonal (t) phase with space group

B. Prasad
Department of Materials Engineering
Indian Institute of Science
Bangalore, Karnataka 560012, India
R. Ramesh
Department of Physics
University of California
Berkeley, CA 94720, USA
R. Ramesh
Department of Materials Science and Nanoengineering
Rice University
Houston, TX 77005, USA
R. Ramesh
Department of Physics
Rice University
Houston, TX 77005, USA

© 2024 The Author(s). Advanced Electronic Materials published by Wiley-VCH GmbH

2199160x, 0, Downloaded from https://onlinelibrary.wiley.com/doi/10.1002/aelm.202300877 by Test, Wiley Online Library on [23/07/2024]. See the Terms and Conditions (https://onlinelibrary.wiley.com/terms-and-conditions) on Wiley Online Library for rules of use; OA articles are governed by the applicable Creative Commons License

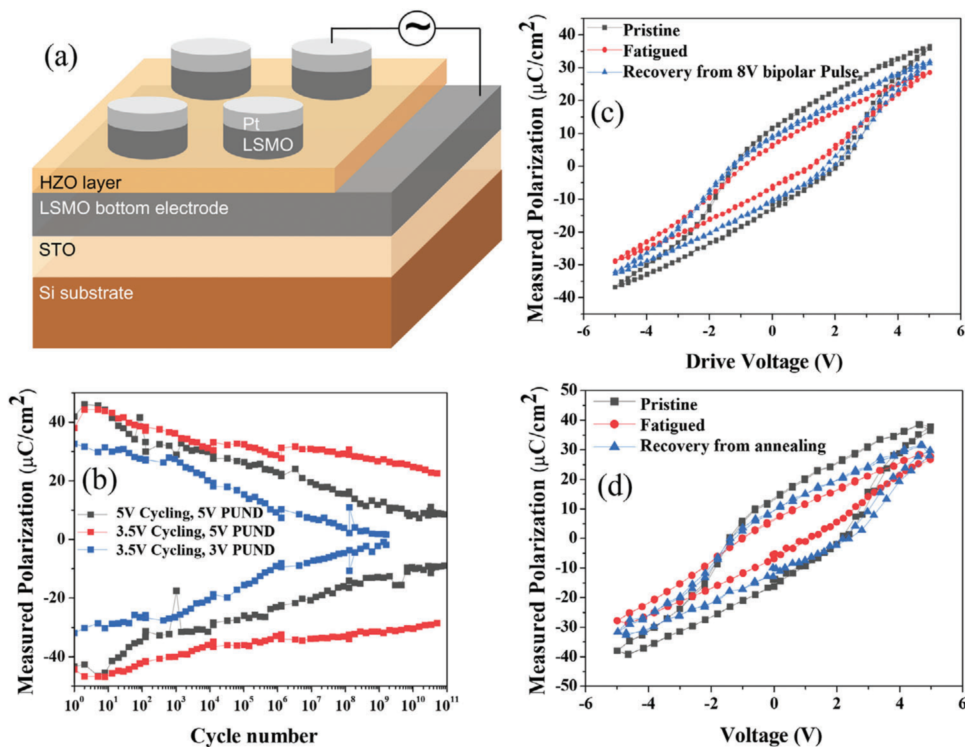

Figure 1. a) Schematic of the HZO capacitor structure and the endurance test; b) Fatigue of HZO capacitors when cycling & testing under different peak voltages; c) The fatigued capacitor partially recovered after applying one electric pulse with higher voltage; d) The fatigued capacitor partially recovered after annealing 1 h at 400 °C in Air.

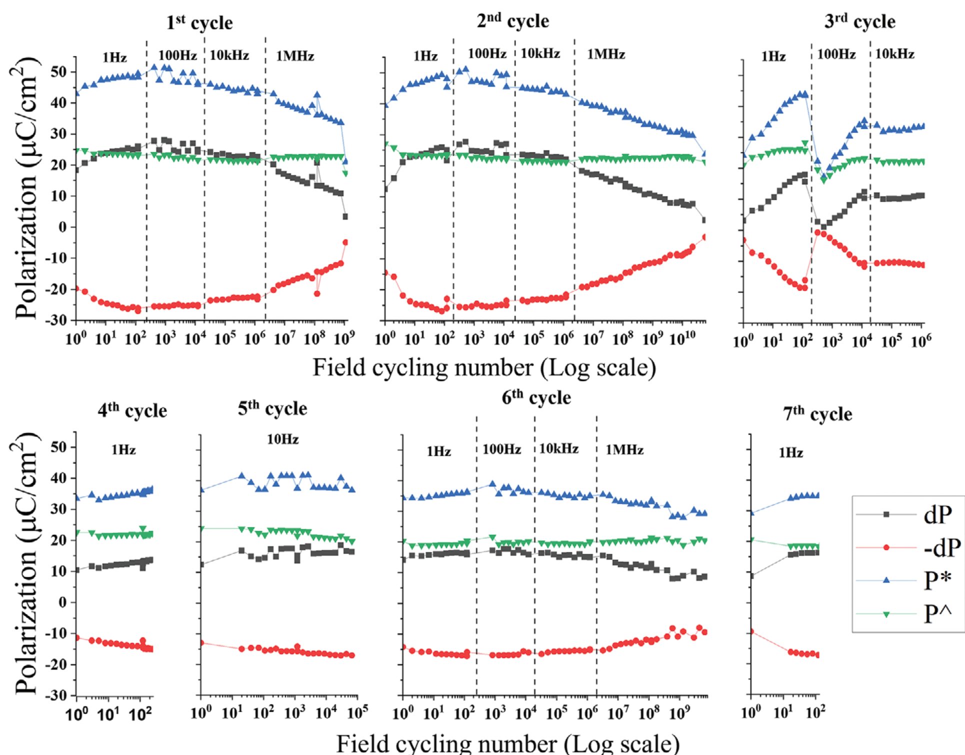

Figure 2. The fatigued HZO capacitor can "wake up" again when cycling at low frequency, indicating there is domain depinning due to oxygen vacancy motion. After a few wakeups and fatigues, the polarization maintains a stable value lower than the initial polarization, suggesting a fatigue mechanism beyond domain pinning.

© 2024 The Author(s). Advanced Electronic Materials published by Wiley-VCH GmbH

2199160x, 0, Downloaded from https://onlinelibrary.wiley.com/doi/10.1002/aelm.202300877 by Test, Wiley Online Library on [23/07/2024]. See the Terms and Conditions (https://onlinelibrary.wiley.com/terms-and-conditions) on Wiley Online Library for rules of use; OA articles are governed by the applicable Creative Commons License

ADVANCED ELECTRONIC MATERIALS Open Access
www.advelectronicmat.de

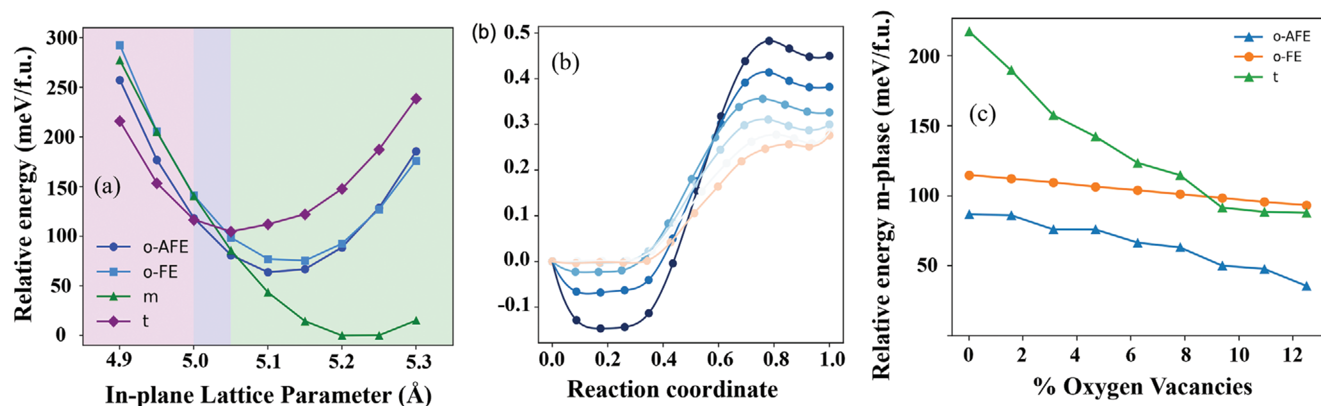

Figure 3. a) Relative energies of the m-, t-, o-AFE, and o-FE phases of $Hf_{0.5}Zr_{0.5}O_2$ calculated from DFT with in-plane epitaxial strain. b) Nudged-elastic band calculations of the o-HZO to t-HZO transition for epitaxial strain values of −1%, 0%, and +1%. c) Relative energies of the t, o-AFE, and o-FE phases with oxygen vacancy concentration relative to that of the m phase.

P4/nmm. For this, HZO had a 50:50 Hf:Zr stoichiometry adopting a checkerboard alloy composition of the cation sublattice (that is, Hf and Zr alternating in all directions) and a unit cell comprised of 32 formula units (98 atoms) to allow for a range of low-concentration oxygen vacancies to be explored. We found that different alloy orderings have energy differences (≈meV/f.u.) less than those between the different polymorphs (≈10 meV per f.u.), so consider only this checkerboard ordering for this work. Consistent with prior work we find that the m-phase is the ground state structure, while other polymorphs are accessible with strain (**Figure 3a**). A small compressive strain favors the o-AFE phase, and the t-phase is favored at higher strain values. Interestingly, and as has been previously noted, the o-FE is never the global ground state even with applied strain.

We argue that this irreversible effect leading to the fatigue behavior of HZO arises from the phase transformation from the polar o-phase to the nonpolar m-phase. According to the density functional theory (DFT) calculations described later, while the o- to t- and o- to m-phase pathways are initially energetically competitive, the m-phase is globally far more stable and cannot be recovered once adopted. We now present experimental evidence for the increased presence of the m-phase during switching cycles, and following that, connect it to our theoretical analysis.

The structural phase transition during the fatigue process was investigated by scanning X-ray nano-diffraction. Unlike other local or bulk characterization methods, the nanoscale X-ray beam, with a resolution down to ≈30 nm, can easily locate and map out the reciprocal space information of each device. Three states of the capacitor are scanned for structural information: pristine, after wake-up, and after a fully fatigued state. The diffraction peak intensity of the nonpolar monoclinic phase and the polar orthorhombic phase are integrated to estimate the phase ratio on the capacitors. This semi-quantitative result is shown in **Figure 4b**: As more electric cycles are applied, from the pristine to the wake-up state, until the fatigue state, the m-/o-phase ratio keeps increasing, demonstrating the phase transition from o- to m-phase is a fundamental cause of the degradation of HZO ferroelectricity. Semi-quantitative analysis of m-/o- phase ratio and higher resolution nanodiffraction images are listed in the supplementary Figure S2 (Supporting Information). This result is consistent with past experimental findings and assumptions about HZO fatigue.[31] We also find that the o-phase fraction is reduced in the wake-up state compared to the pristine state, which indicates the polarization increase is not primarily caused by increasing polar phase, providing evidence that domain depinning is the leading cause of the wake-up effect instead of phase transition. Such contributions of domain depinning in the wake-up process have been previously reported in HZO systems.[31–33]

To investigate another possible phase switching of t- to m-phase, we consider the kinetic energy barriers for the phase transition in going from t- to m- and t- to o-phase. Prior reports of these barriers range from 208 to 315 meV per formula unit (f.u.) for the t- to m-phase transition, and 22 to 31 meV per f.u. for the t- to o-phase transition. From these observations, we can infer that the phase transition from t- to m-phase is kinetically suppressed, despite the m-phase being the global ground-state polymorph. However, while the t-phase to o-phase transition is more favorable than the t-phase to m-phase from these kinematic considerations, an interesting result emerges when we consider repeated switching cycles. Instead, for the reverse transition, the large barrier that disfavors the t- to m-phase transition, now acts as a stabilizing force for the m-phase. The result of this is that repeated cycling will gradually increase the volume fraction of the m-phase, consistent with our experimental results. Finally, we explore the role of strain on the t- to o-phase barrier by performing nudged elastic band calculations for several values of compressive and tensile strain (Figure 3b). Consistent with prior reports,[13,34] we find that strain can indeed modify the barrier heights for this phase transition. However, it does not increase it to a level such that it would be competitive with the t-phase to m-phase transition. In fact, we find that for small amounts of tensile strain, the t- to o-phase barrier is reduced, favoring a greater volume fraction of the polar phase, as has been observed in the literature.

The oxygen vacancy plays an essential role in the HZO phase transition, and as we hypothesize, in its fatigue behavior. Prior work[24] observed the structural change of the LSMO electrode between perovskite and brownmillerite with an applied electric bias to the LSMO/HZO/LSMO stack. Their findings demonstrated that a significant volume of oxygen vacancies migrate through the interface under an electric field, with the LSMO electrode

© 2024 The Author(s). Advanced Electronic Materials published by Wiley-VCH GmbH
2199160x, 0, Downloaded from https://onlinelibrary.wiley.com/doi/10.1002/aelm.202300877 by Test, Wiley Online Library on [23/07/2024]. See the Terms and Conditions (https://onlinelibrary.wiley.com/terms-and-conditions) on Wiley Online Library for rules of use; OA articles are governed by the applicable Creative Commons License

2199160x, 0, Downloaded from https://onlinelibrary.wiley.com/doi/10.1002/aelm.202300877 by Test, Wiley Online Library on [23/07/2024]. See the Terms and Conditions (https://onlinelibrary.wiley.com/terms-and-conditions) on Wiley Online Library for rules of use; OA articles are governed by the applicable Creative Commons License

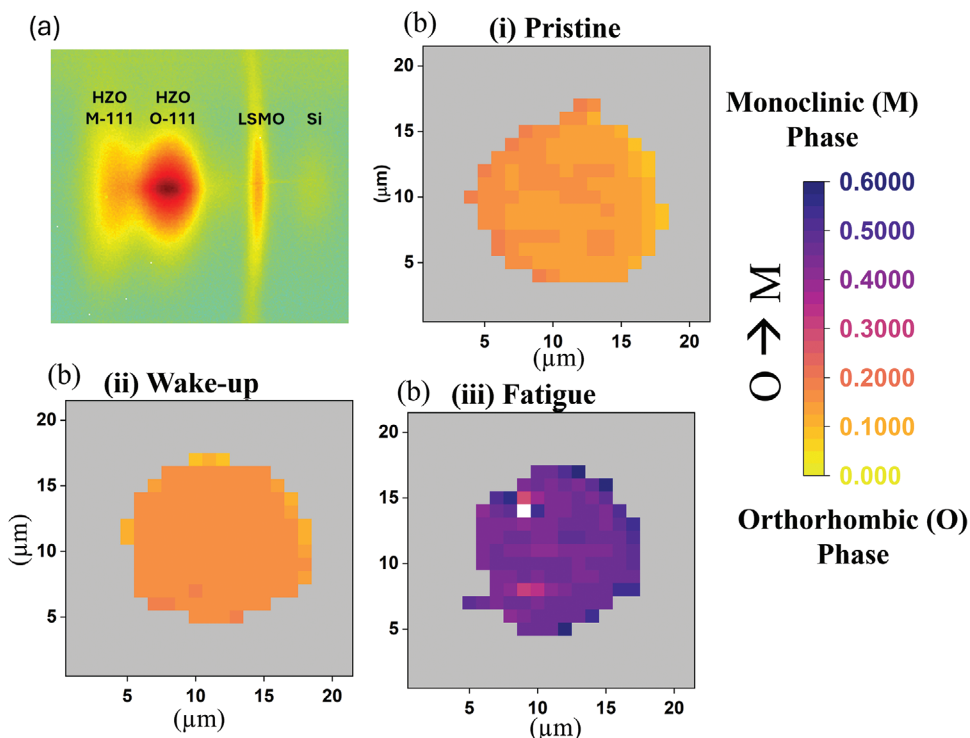

Figure 4. X-ray nano-diffraction of single capacitors at different fatigue states. a) the diffraction pattern of a 1 μm × 1 μm area. b) Scanning of capacitors at three different states: pristine, wake-up, and fatigue. The figure shows the diffraction intensity ratio of the non-ferroelectric, monoclinic phase to the ferroelectric, orthorhombic phase. The ratio keeps increasing from the pristine to the fatigued state, indicating a phase transition from the o- to the m-phase during cycling.

concurrently functioning as both a source and sink for oxygen vacancies. Thus, there is a constant process of oxygen vacancy redistribution during field cycling. Another research involving an IrO_2 electrode suggests that an increase in oxygen content within HZO correlates with a higher proportion of the m-phase.[35] It is hypothesized that oxygen vacancy redistribution within the HZO/LSMO system could result in an increase in oxygen within the HZO film, thereby promoting the m-phase within HZO. Supporting this, as demonstrated in prior work,[12,32,33,36–38] and corroborated by our own DFT calculations, oxygen vacancies do reduce the barrier to obtaining the polar o-AFE and o-FE phases relative to the m-phase (Figure 3c). Therefore, one key conclusion is that having a readily available source/sink of oxygen vacancies is crucial for obtaining and maintaining the o-phase regions. Thus, during cycling, if the HZO becomes further oxygenated (i.e., depleted of oxygen vacancies) as they migrate and are pinned at domain walls, it will result in a reduction in the volume fraction of the o-phase and consequently a reduction in the polarization.

To further explore the influence of oxygen vacancy concentration on fatigue behavior, we reduced the concentration of mobile oxygen vacancies by doping HZO with 0.7% La (corresponding to ≈10^{20} cm^{-3} concentration). Our hypothesis of doping with La is that since the oxygen vacancies tend to bind to the La^{3+}, there will be less migration/redistribution of the oxygen vacancies in La:HZO than in pure HZO. Because of this, domain wall pinning by oxygen vacancies will be suppressed in La:HZO. After the same etching and testing process, we compare the fatigue rate of pure HZO and La:HZO in Figure 2. The endurance lifetime of these La:HZO capacitors (Figure S1, Supporting Information) is measurably higher compared to HZO devices (Figure 2), consistent with our expectations as well as the past report.[39] This result supports the notion that maintaining a stable oxygen vacancy concentration level is crucial in preserving ferroelectricity in HZO.

In summary, we present direct structural evidence, supported by ab initio calculations that point to the role of oxygen intercalation into the o-phase of HZO to destabilize it into the nonpolar m-phase. This mechanism is pointedly different from that in the perovskite ferroelectrics such as PZT. Thus, we surmise that a precise defect in chemistry engineering leads to the trapping of the oxygen vacancies (and thus the stability of the o-phase) in the HZO structure sandwiched by oxide electrodes.

2. Material System and Characterization Methods

2.1. Deposition and Fabrication of HZO Capacitor Stacks

The 30 nm $La_{0.67}Sr_{0.33}MnO_3$/10 nm $Hf_{0.5}Zr_{0.5}O_2$/45 nm $La_{0.67}Sr_{0.33}MnO_3$ thin film stacks were deposited on 001-oriented $SrTiO_3$ coated Si substrates by pulsed laser deposition using a KrF excimer laser (248 nm, LPX 300, Coherent). The growth of all layers was carried out in a dynamic oxygen pressure of 100mTorr, at a growth temperature of 600 °C, and laser fluence of 1.0 J cm^{-2}. The laser repetition rate for LSMO and HZO growth are 4 and 2 Hz respectively. Following growth, the samples were cooled to room temperature at a cooling rate of

© 2024 The Author(s). Advanced Electronic Materials published by Wiley-VCH GmbH

10 °C min^{-1} under a static oxygen pressure of 1 atm. The circular capacitors (12.5 μm in diameter) were then fabricated using the photolithography and Ar ion milling method.

2.2. X-Ray Nano Diffraction

The X-ray nano diffraction was performed in section 26-ID-C of Advanced Photon Source, Argonne National Laboratory. The X-ray beam was 10 keV with a beam size of 30 nm. The motors of the sample stage and the detector provide 4D maps (2D in real space and 2D in reciprocal space) with high accuracy.

2.3. Electrical Characterization

Ferroelectric polarization hysteresis loops and PUND measurements were measured at room temperature using a Precision Multiferroic Tester (Radiant Technologies). The hysteresis measurements were completed at a frequency of 10 kHz. The pulse width and delay of PUND measurements are 10 μs and 0.1 s.

2.4. DFT Calculations

Density functional theory (DFT) calculations were performed at the Generalized-Gradient Approximation (GGA) level using the Vienna ab initio simulation package.[40,41] The PBE exchange-correlation function[42,43] was used along with a 6 × 6 × 6 Monkhorst packing k-point grid, 500 eV plane-wave cutoff, and projector-augmented wave (PAW) pseudopotentials.[44–46] Valence sets of 6s5d, 4s4p5s4d, and 2s(2)2p(4) were used for hafnium, zirconium and oxygen respectively.

Energy landscapes for the displacive phase transitions between orthorhombic and tetragonal $Hf_{0.5}Zr_{0.5}O_2$ (HZO) were conducted using the nudged elastic band (NEB) method, as implemented in the VASP Transition State Tools (TST) software.[47,48] All NEB calculations were optimized starting from a linear interpolation, and intermediate images were optimized to a force tolerance of (0.005 eV Å^{-1}) using the quick-min algorithm.[49] For the epitaxial strained structures, only the cell positions were optimized, while otherwise the ssNEB algorithm[50] was used to optimize cell volume and shape as well.

Epitaxial strain calculations were performed by fixing the in-plane lattice parameters and allowing the out-of-plane lattice parameter and internal coordinates to optimize.

Supporting Information

Supporting Information is available from the Wiley Online Library or from the author.

Acknowledgements

Z.Z. and R.R. acknowledge funding support from Western Digital. R.R. acknowledges partial support from the U.S. Department of Energy, Office of Science, Office of Basic Energy Sciences, Materials Sciences and Engineering Division under Contract No. DE-AC02-05-CH11231 (Codesign of Ultra-Low-Voltage Beyond CMOS Microelectronics for the development of materials for low-power microelectronics). This research used resources of the Advanced Photon Source (26-ID-C), a U.S. Department of Energy (DOE) Office of Science user facility operated for the DOE Office of Science by Argonne National Laboratory under Contract No. DE-AC02-06CH11357. B. P. acknowledges the funding support from the ISRO-IISc Space Technology Cell, Indian Institute of Science.

Conflict of Interest

The authors declare no conflict of interest.

Data Availability Statement

The data that support the findings of this study are available in the supplementary material of this article.

Keywords

fatigue, ferroelectric, field-cycling, hafnia, phase transformation

Received: December 15, 2023
Revised: May 11, 2024
Published online:

[1] D. Das, A. I. Khan, *IEEE Nanotechnol. Mag.* **2021**, *15*, 20.
[2] S. Jeon, *ECS Trans.* **2020**, *98*, 219.
[3] Q. Luo, Y. Cheng, J. Yang, R. Cao, H. Ma, Y. Yang, R. Huang, W. Wei, Y. Zheng, T. Gong, J. Yu, X. Xu, P. Yuan, X. Li, L. Tai, H. Yu, D. Shang, Q. Liu, B. Yu, Q. Ren, H. Lv, M. Liu, *Nat. Commun.* **2020**, *11*, 1391.
[4] T. Schenk, S. Mueller, presented at *IEEE Int. Symp. Appl. Ferroelectr*, Sydney, Australia, July, **2021**.
[5] U. Schroeder, C. S. Hwang, H. Funakubo, in *Ferroelectricity in Doped Hafnium Oxide: Materials, Properties and Devices*, Woodhead Publishing, Sawston, UK, **2019**.
[6] F. Fengler, M. H. Park, T. Schenk, M. Pešić, U. Schroeder, in *Ferroelectricity in Doped Hafnium Oxide: Materials Properties and Devices*, (Eds: U. Schroeder, C. S. Hwang, H. Funakubo), Woodhead Publishing, Sawston, UK, **2019**, ch. 9.2.
[7] Y. Goh, S. H. Cho, S.-H. K. Park, S. Jeon, *Nanoscale* **2020**, *12*, 9024.
[8] W. Hamouda, F. Mehmood, T. Mikolajick, U. Schroeder, T. O. Mentes, A. Locatelli, N. Barrett, *Appl. Phys. Lett.* **2022**, *120*, 202902.
[9] M. G. Kozodaev, A. G. Chernikova, E. V. Korostylev, M. H. Park, R. R. Khakimov, C. S. Hwang, A. M. Markeev, *J. Appl. Phys.* **2019**, *125*, 034101.
[10] M. Pešić, F. P. G. Fengler, L. Larcher, A. Padovani, T. Schenk, E. D. Grimley, X. Sang, J. M. LeBeau, S. Slesazeck, U. Schroeder, T. Mikolajick, *Adv. Funct. Mat.* **2016**, *26*, 4601.
[11] W. Wei, W. Zhang, F. Wang, X. Ma, Q. Wang, P. Sang, X. Zhan, Y. Li, L. Tai, Q. Luo, H. Lv, J. Chen, *IEEE Int. Electron Devices Meet*, San Francisco, CA, USA, March, **2020**.
[12] M. Hoffmann, U. Schroeder, T. Schenk, T. Shimizu, H. Funakubo, O. Sakata, D. Pohl, M. Drescher, C. Adelmann, R. Materlik, A. Kersch, T. Mikolajick, *J. Appl. Phys.* **2015**, *118*, 072006.
[13] B. Johnson, J. L. Jones, in *Ferroelectricity in Doped Hafnium Oxide: Materials Properties and Devices*, (Eds: U. Schroeder, C.S. Hwang, H. Funakubo), Woodhead Publishing, Sawston, UK, **2019**, ch. 2.
[14] J. Lowther, J. Dewhurst, J. Leger, J. Haines, *Phys. Rev. B* **1999**, *60*, 14485.
[15] S. J. Kim, D. Narayan, J.-G. Lee, J. Mohan, J. S. Lee, J. Lee, H. S. Kim, Y.-C. Byun, A. T. Lucero, C. D. Young, *Appl. Phys. Lett.* **2017**, *111*, 242901.

© 2024 The Author(s). Advanced Electronic Materials published by Wiley-VCH GmbH

2199160x, 0, Downloaded from https://onlinelibrary.wiley.com/doi/10.1002/aelm.202300877 by Test, Wiley Online Library on [23/07/2024]. See the Terms and Conditions (https://onlinelibrary.wiley.com/terms-and-conditions) on Wiley Online Library for rules of use; OA articles are governed by the applicable Creative Commons License

[16] M. H. Park, Y. H. Lee, H. J. Kim, Y. J. Kim, T. Moon, K. D. Kim, S. D. Hyun, T. Mikolajick, U. Schroeder, C. S. Hwang, *Nanoscale* **2017**, *10*, 716.
[17] M. H. Park, T. Schenk, C. S. Hwang, U. Schroeder, in *Ferroelectricity in Doped Hafnium Oxide: Materials Properties and Devices*, (Eds: U. Schroeder, C.S. Hwang, H. Funakubo), Woodhead Publishing, Sawston, UK, **2019**, ch. 8.
[18] F. Chen, Q. Z. Liu, H. F. Wang, F. H. Zhang, W. Wu, *Appl. Phys. Lett.* **2007**, *90*, 192907.
[19] C. W. Law, K. Y. Tong, J. H. Li, K. Li, M. C. Poon, *Thin Solid Films* **1999**, *354*, 162.
[20] J. Lee, R. Ramesh, V. G. Keramidas, W. L. Warren, G. E. Pike, J. T. Evans, *Appl. Phys. Lett.* **1995**, *66*, 1337.
[21] R. Ramesh, H. Gilchrist, T. Sands, V. G. Keramidas, R. Haakenaasen, D. K. Fork, *Appl. Phys. Lett.* **1993**, *63*, 3592.
[22] Y. Wei, P. Nukala, M. Salverda, S. Matzen, H. J. Zhao, J. Momand, A. S. Everhardt, G. Agnus, G. R. Blake, P. Lecoeur, B. J. Kooi, J. Iniguez, B. Dkhil, B. Noheda, *Nat. Mater.* **2018**, *17*, 1095.
[23] B. Prasad, V. Thakare, A. Kalitsov, Z. Zhang, B. Terris, R. Ramesh, *Adv. Electroton. Mater.* **2021**, *7*, 2001074.
[24] P. Nukala, M. Ahmadi, Y. Wei, S. de Graaf, E. Stylianidis, T. Chakrabortty, S. Matzen, H. W. Zandbergen, A. Björling, D. Mannix, D. Carbone, B. Kooi, B. Noheda, *Science* **2021**, *372*, 630.
[25] J. Lyu, T. Song, I. Fina, F. Sánchez, *Nanoscale* **2020**, *12*, 11280.
[26] X. J. Lou, *J. Appl. Phys.* **2009**, *105*, 024101.
[27] J. F. Scott, M. Dawber, *Appl. Phys. Lett.* **2000**, *76*, 3801.
[28] I. K. Yoo, S. B. Desu, *Phys. Status Solidi A* **1992**, *133*, 565.
[29] P. Kofstad, D. J. Ruzicka, *J. Electrochem. Soc.* **1963**, *110*, 181.
[30] M. F. Trubelja, V. S. Stubican, *Solid State Ionics* **1991**, *49*, 89.
[31] S. S. Fields, S. W. Smith, P. J. Ryan, S. T. Jaszewski, I. A. Brummel, A. Salanova, G. Esteves, S. L. Wolfley, M. D. Henry, P. S. Davids, J. F. Ihlefeld, *ACS Appl. Mater. Interfaces* **2020**, *12*, 26577.
[32] M. Pešić, F. P. G. Fengler, L. Larcher, A. Padovani, T. Schenk, E. D. Grimley, X. Sang, J. M. LeBeau, S. Slesazeck, U. Schroeder, T. Mikolajick, *Adv. Funct. Mater.* **2016**, *26*, 4601.
[33] T. Gong, J. Li, H. Yu, Y. Xu, P. Jiang, Y. Wang, P. Yuan, Y. Wang, Y. Chen, Y. Ding, Y. Yang, Y. Wang, B. Chen, Q. Luo, *IEEE Electron Device Lett.* **2021**, *42*, 1288.
[34] Z. Zhang, S.-L. Hsu, V. A. Stoica, H. Paik, E. Parsonnet, A. Qualls, J. Wang, L. Xie, M. Kumari, S. Das, Z. Leng, M. McBriarty, R. Proksch, A. Gruverman, D. G. Schlom, L.-Q. Chen, S. Salahuddin, L. W. Martin, R. Ramesh, *Adv. Mater.* **2021**, *33*, 2006089.
[35] T. Mittmann, T. Szyjka, H. Alex, M. C. Istrate, P. D. Lomenzo, L. Baumgarten, M. Müller, J. L. Jones, L. Pintilie, T. Mikolajick, Uwe Schroeder, *Rapid Res. Lett.* **2021**, *15*, 2100012.
[36] H.-J. Lee, M. Lee, K. Lee, J. Jo, H. Yang, Y. Kim, S. C. Chae, U. Waghmare, J. H. Lee, *Science* **2020**, *369*, 1343.
[37] L. Azevedo Antunes, R. Ganser, U. Schroeder, T. Mikolajick, A. Kersch, *Adv. Mater. Interfaces* **2024**, *11*, 2300710.
[38] M. Materano, P. D. Lomenzo, A. Kersch, M. H. Park, T. Mikolajick, U. Schroeder, *Inorg. Chem. Front.* **2021**, *8*, 2650.
[39] A. G. Chernikova, M. G. Kozodaev, D. V. Negrov, E. V. Korostylev, M. H. Park, U. Schroeder, C. S. Hwang, A. M. Markeev, *ACS Appl. Mater. Interfaces* **2018**, *10*, 2701.
[40] J. Hafner, *J. Comput. Chem.* **2008**, *29*, 2044.
[41] G. Kresse, J. Furthmüller, *Phys. Rev. B* **1996**, *54*, 11169.
[42] J. P. Perdew, K. Burke, M. Ernzerhof, *Phys. Rev. Lett.* **1996**, *77*, 3865.
[43] J. P. Perdew, Y. Wang, *Phys. Rev. B* **1992**, *46*, 12947.
[44] P. E. Blöchl, *Phys. Rev. B* **1994**, *50*, 17953.
[45] G. Kresse, D. Joubert, *Phys. Rev. B* **1999**, *59*, 1758.
[46] D. Vanderbilt, *Phys. Rev. B* **1990**, *41*, 7892.
[47] G. Henkelman, H. Jónsson, *J. Chem. Phys.* **2000**, *113*, 9978.
[48] H. Jónsson, G. Mills, K. W. Jacobsen, B. J. Berne, G. Ciccotti, D. F. Coker, in *Classical And Quantum Dynamics In Condensed Phase Simulations*, world scientific publishing, Singapore, **1998**.
[49] D. Sheppard, R. Terrell, G. Henkelman, *J. Chem. Phys.* **2008**, *128*, 134106.
[50] D. Sheppard, P. Xiao, W. Chemelewski, D. D. Johnson, G. Henkelman, *J. Chem. Phys.* **2012**, *136*, 074103.

© 2024 The Author(s). Advanced Electronic Materials published by Wiley-VCH GmbH

2199160x, 0, Downloaded from https://onlinelibrary.wiley.com/doi/10.1002/aelm.202300877 by Test, Wiley Online Library on [23/07/2024]. See the Terms and Conditions (https://onlinelibrary.wiley.com/terms-and-conditions) on Wiley Online Library for rules of use; OA articles are governed by the applicable Creative Commons License